Origins for the Near-Earth Asteroids

Richard P. Binzel,* Shui Xu, Schelte J. Bus, Edward Bowell

Because of their short dynamical lifetimes, the population of near-Earth asteroids (NEAs) must be resupplied. Two sources have been hypothesized: main-belt asteroids and extinct comet nuclei. The difficulty of making physical measurements for similar sized (diameter D less than 5 kilometers) main-belt asteroids and comet nuclei has limited comparative tests for distinguishing between these alternatives. A new survey of physical properties for $D < 5$ kilometers main-belt asteroids reveals that their spin rate and shape distributions are similar to those of NEAs, as is fully consistent with a main-belt origin for most NEAs. Physical data on comet nuclei are limited. If the existing sample is representative of the comet population, analysis of the asteroid and comet samples constrains the fraction of comet nuclei to between 0 and 40 percent of the total NEA population.

Objects in near-Earth space (*1*), comprising asteroids and active comets, as well as dormant or extinct comet nuclei, have dynamical lifetimes substantially shorter than the age of the solar system. Over time scales of 10^7 to 10^8 years, they are removed either by planetary gravitational interactions leading to their ejection from the solar system or by collisions with the terrestrial planets (*2*). The latter removal mechanism may have a significant effect on biological evolution on Earth (*3*). By virtue of their current existence and the terrestrial planet cratering record, near-Earth objects must have some continual source of resupply. Two sources have been proposed: asteroids from the main-belt and extinct or dormant comet nuclei (*4, 5*). Here we report on new observational results that allow the relative contributions from these two populations to be examined by comparing their physical properties.

By present convention, objects discovered in near-Earth space that maintain a stellar appearance are classified as asteroids; we refer to these objects as near-Earth asteroids (NEAs), recognizing that objects of both asteroidal and cometary genesis could be included in this population. About 200 NEAs have been discovered, out of an estimated population of up to 10^4 objects larger than 0.5 km in diameter. They are categorized according to their orbital elements as Atens, Apollos, and Amors (*6*). Aten and Apollo asteroids have orbits that cross the Earth's, whereas Amor asteroids have perihelia just beyond the Earth's aphelion. Nearly all known NEAs have diameters less than 5 km, with two notable exceptions, 433 Eros and 1036 Ganymed, which have diameters of about 20 and 40 km, respectively. Although NEAs are small, their close approaches to the Earth allow many of them to reach sufficiently bright apparent magnitudes to allow telescopic measurements of their physical properties (*7*). These measurements include taxonomic classification of their spectral properties as well as measurements of their rotation rates and approximate shapes.

However, a comparison of the physical properties of main-belt and NEAs has been problematic (*8*). A primary difficulty has been the challenge of obtaining physical measurements for main-belt asteroids in the same size range as that of the near-Earth objects. Generally, their greater distances and fainter apparent magnitudes have limited physical studies of main-belt asteroids to those with diameters greater than 30 km. A few dedicated surveys and analyses of physical properties have been made for asteroids smaller than 30 km in diameter (*8, 9*), but the mean diameters of these main-belt samples are a factor of 4 or more larger than the NEA sample, corresponding to a difference in mass of nearly two orders of magnitude.

We therefore undertook a new survey (*10*) to measure the physical properties of main-belt asteroids having sizes and masses comparable to those of the observed NEAs. To achieve this goal, we used charge-coupled-device (CCD) detectors on the 1.8-m telescope at the Anderson Mesa, Arizona, facility of Lowell Observatory and on the 1.3- and 2.4-m telescopes of the Michigan Dartmouth MIT Observatory at Kitt Peak, Arizona. The CCD imaging observations of 32 small main-belt asteroids having diameters of ~5 km or less were conducted on 50 nights from November 1987 through May 1991. Two of these objects were serendipitous new discoveries within the main-belt (*10*). In addition, one new Trojan asteroid orbiting at the L5 Lagrange point of Jupiter was discovered.

Brightness variations for each program asteroid were measured through repeated imaging, usually for more than 6 hours on each of two or more nights. Typical exposure times of 300 or 600 s allowed photometric precision of 1 to 2% to be achieved down to a magnitude of $V = 19$, corresponding to a ~2 km object in the inner main belt. Brightness variations resulting from atmospheric extinction were removed by differencing all asteroid measurements with respect to measurements of a set of two to three comparison stars imaged simultaneously in the CCD frame. Absolute calibration was achieved through near-simultaneous imaging of standard stars on photometric nights.

Intrinsic periodic variations in an asteroid's brightness (Figs. 1 and 2) reveal its synodic rotation period, and the amplitude

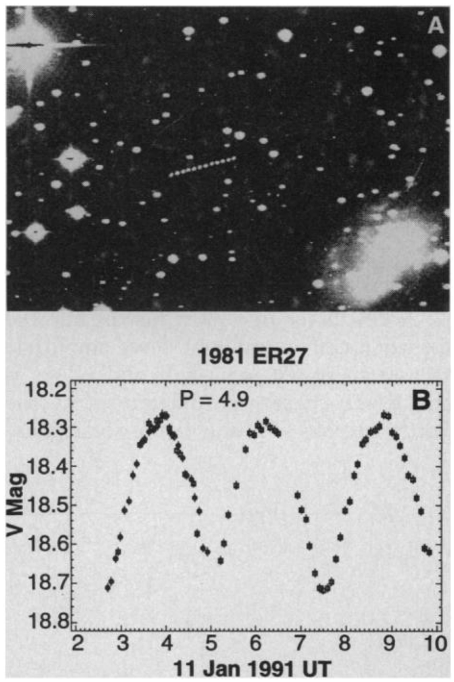

Fig. 1. (**A**) A composite image of 12 separate CCD frames obtained on universal time (UT) 11 January 1991 containing the 2-km diameter main-belt asteroid 1981 ER27. Each frame consisted of a 300-s exposure using a TI-4849 CCD attached to the 1.3-m McGraw-Hill telescope at the Michigan Dartmouth MIT Observatory located on Kitt Peak, Arizona. The field size is 3 by 4.6 arc min. North is to the top and west is to the left. The asteroid's motion was from northeast to southwest. The diffuse object in the southeast corner of the field is the galaxy UGC 03390. (**B**) Photometric measurements extracted from repetitive imaging as shown in (A) are used to determine the rotational light curve for the target asteroid. The abscissa is in units of hours and the ordinate is in units of stellar magnitudes. A periodic variation with two maxima and two minima per cycle reveals a 4.9-hour rotation period (P) (equivalently 4.90 rev/day) for asteroid 1981 ER27 with a peak-to-peak amplitude of 0.46 magnitudes. Data obtained after 7.5 hours UT have been replotted with a different symbol (circle) one cycle earlier to show the quality of the period solution.

R. P. Binzel and S. Xu, Department of Earth, Atmospheric, and Planetary Sciences, Massachusetts Institute of Technology, Cambridge, MA 02139.
S. J. Bus and E. Bowell, Lowell Observatory, Flagstaff, AZ 86001.
*To whom correspondence should be addressed.

(measured from minimum to maximum brightness) is diagnostic of its shape. For a uniform density triaxial ellipsoid with axes $a > b > c$ rotating about its principal axis c, an observer orthogonal to the spin vector would measure two maxima and minima per complete rotation, where the ratio of the intensities for a body with a geometrically scattering, fully illuminated surface is a simple measure of a/b. In reality, however, asteroids are not perfect geometrically scattering ellipsoids, illumination angles vary, and the orientations of the spin vectors are generally unknown. Thus careful corrections must be applied when comparing samples of asteroid rotational properties to achieve a meaningful physical analysis.

We compared (Table 1) data for main-belt objects from the small main-belt asteroid survey (*10*) and for NEAs and comets from other sources (*7, 9, 11, 12*). The large NEAs 433 Eros and 1036 Ganymed were excluded because they are pronounced outliers from the diameter distribution of the remainder of the population. The tabulated mean rotational frequency (revolutions per day) is for the assumption that each object displays two maxima and minima per rotation.

A key factor that must first be allowed for when comparing light curve amplitude measurements of main-belt and NEAs is the effect caused by differences in the Earth-asteroid-Sun angle (the solar phase angle) at which the observations were made (*13*). Because of their proximity, NEAs are more likely to be observed at large phase angles (often exceeding 50°). Main-belt asteroids are observable over a much narrower range; most observations have been performed at phase angles less than 15°. To account for the effects of increasing light curve amplitude with increasing phase angle, we used empirical relations (*14*) to correct amplitude measurements to a phase angle of 0°. These corrections were applied to all original data for the samples listed in Table 1.

A second factor that can affect the observed amplitude for a NEA is a change in aspect angle, because the object can traverse a large angular distance across the sky during a single apparition. Under the assumption that the spin vectors of the observed asteroids are all randomly oriented, the aspect angles (measured from the asteroid's pole to the observer's line of sight) are randomly distributed about a mean of 60°. This assumed mean aspect angle is valid for the main-belt asteroid and comet samples in that each object was observed at a single geometry. For NEAs observed over several aspects (commonly involving more than one apparition), the correction procedure developed by Binzel and Sauter (*15*) was applied to estimate the light curve amplitude that would be observed at an aspect angle of 60°. The uncertainties associated with light curve amplitude corrections for solar phase angle and aspect angle are estimated to produce errors in the mean corrected amplitudes (Table 1) that are small compared with natural dispersions intrinsic to the listed standard deviations of the mean.

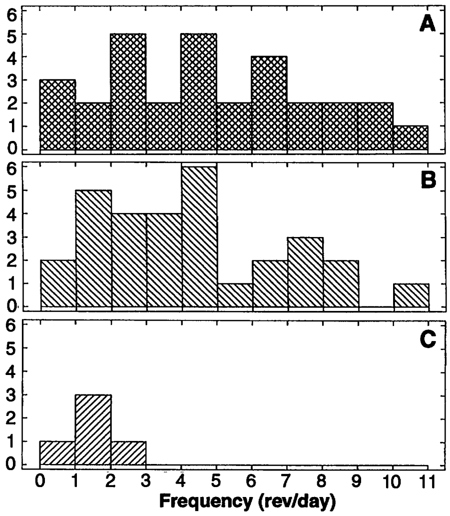

Fig. 3. Histograms showing the rotational frequency distributions for samples of (**A**) NEAs, (**B**) similar-sized (D < 5 km) small main-belt asteroids, and (**C**) comet nuclei. Both asteroid samples show similar dispersions and have similar means. Although rotation rates of comet nuclei fall within the observed range for asteroids, their mean rotational frequency is significantly different.

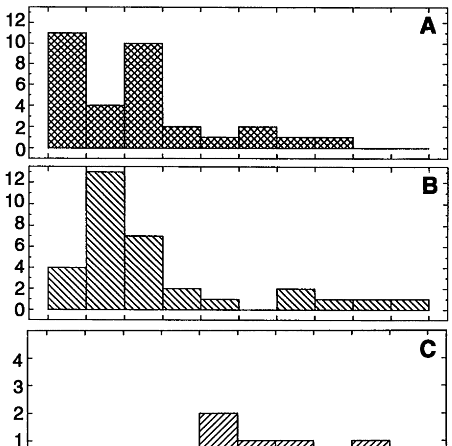

Fig. 4. Histograms showing the light curve amplitude distributions for samples of (**A**) NEAs, (**B**) similar-sized (D < 5 km) small main-belt asteroids, and (**C**) comet nuclei. All samples have been corrected for phase angle and aspect effects. Both asteroid samples show similar dispersions and have similar means. Although comet nuclei measurements fall within the observed range for asteroids, their mean corrected amplitude is significantly different.

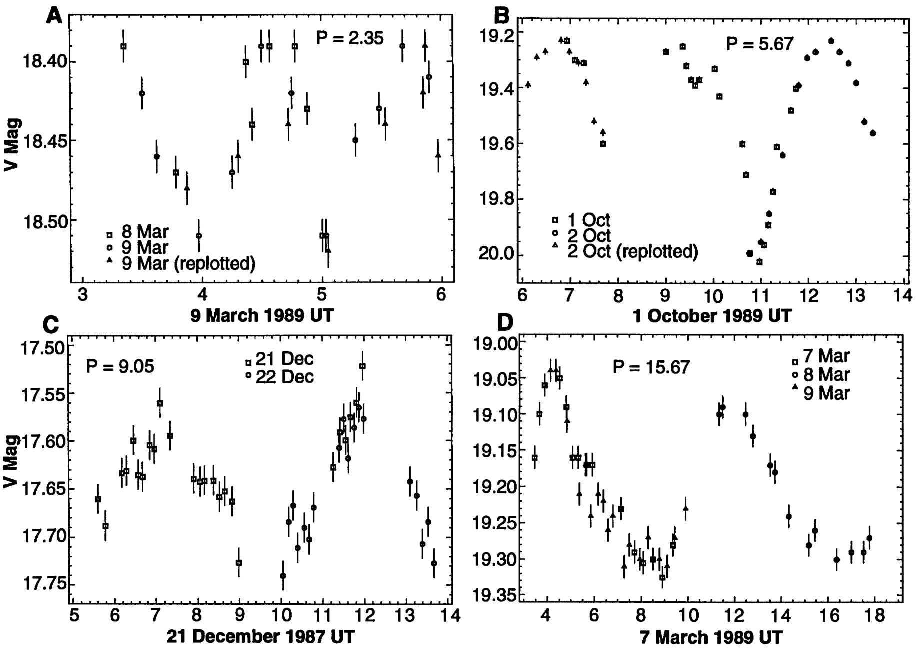

Fig. 2. Four asteroid light curves representative of the range of results found in the small main-belt asteroid light curve survey (*10*). The legends indicate the nights of observation and the rotational period (P, in hours) used to place the data in phase on the UT date labeled on the abscissa. The designation, rotation frequency (f, in revolutions per day) and observed light curve amplitude for each object (A, in magnitudes), respectively, are: (**A**) 1981 ER18, f = 10.2, A = 0.13; (**B**) 1981 EV9, f = 4.23, A = 0.79; (**C**) 1981 EH23, f = 2.65, A = 0.20; (**D**) 1981 EC15, f = 1.53, A = 0.27. All have estimated diameters of about 2 km.

Table 1. Statistical summary of comparison among NEAs (*6, 11*) and small main-belt asteroids (*10*) and comets (*12*). The mean amplitude (in magnitudes, mag) is the value derived from the basic data with no correction for aspect or surface light-scattering. The corrected mean amplitude is explained in the text. In all cases, the listed uncertainty is the standard deviation of the mean. *N*, number of samples; rev, revolutions.

Sample	*N*	Mean diameter (km)	Mean frequency (rev/day)	Mean amplitude (mag)	Corrected mean amplitude (mag)
Near-Earth asteroids	32	3	4.94 ± 0.54	0.482 ± 0.080	0.224 ± 0.032
Small main-belt asteroids	32	3	4.30 ± 0.46	0.307 ± 0.048	0.269 ± 0.041
Comet nuclei	5	11	1.64 ± 0.39	0.670 ± 0.083	0.598 ± 0.081

The observed dispersion in rotation rates (Fig. 3) is quite similar for the small main-belt and near-Earth asteroid samples. The mean rotational frequencies for these two samples are also statistically indistinguishable (Table 1). Similarly, the distributions of the corrected light curve amplitudes are comparable for the small main-belt and NEA samples (Fig. 4), and there is no statistical distinction between the mean corrected amplitudes for these two samples (Table 1).

These comparable distributions provide physical evidence that NEAs are similar to their same-sized counterparts in the main asteroid belt. Formal hypothesis testing shows that we cannot reject the null hypothesis that these two samples are drawn from the same population. Thus our observational results are fully consistent with the proposition that the main asteroid belt serves as the complete source of resupply for the NEA population.

A full evaluation of the relative contribution of cometary nuclei to the NEA population based on a comparison of physical properties is difficult because of the paucity of comet measurements. Those values that are available for comet nuclei show distributions of rotation rates and light curves that are dissimilar to the asteroid samples, as evidenced in Figs. 3 and 4. Although the comet nuclei measurements fall within the range of asteroid values, the mean values for rotational frequency and corrected amplitude are substantially different (Table 1). A formal comparison of the means for the small sample sizes, using the nonparametric Mann-Whitney U test, confirms that the mean values for the comet samples are significantly different from the asteroid samples at greater than 99% confidence level.

Although the dynamics of outgassing and mass loss can lead to slow spin rates and irregular shapes for comets (*16*), we cannot rule out that systematic observational selection is a factor in the apparent differences in light curve properties between comet nuclei and small asteroids. Because rotational parameters for comet nuclei are often derived when comae are present or when the objects are at large distances and have faint apparent magnitudes, the available results could have a selection effect toward objects having large amplitudes and modest rotation periods. Although comet researchers are careful to guard against such selection effects, the statistics of the small sample size for cometary nuclei are sensitive to such factors. The situation will improve with additional measurements of the rotational properties of cometary nuclei (*17*).

A physical effect that we cannot rule out completely as a factor in causing the differences in rotational properties between NEAs and active comets is that comets are spun-up or fragmented through collisional evolution as they evolve toward an asteroidal appearance. However, we consider that this effect is unlikely for at least two reasons: (i) the time scale for substantial evolution of rotational angular momentum of an asteroidal or cometary NEA by collision is long compared to the lifetime before removal; and (ii) collisions with sufficient momentum (which is proportional to velocity, v) to substantially alter the rotation of (presumably) structurally weak comet nuclei would have sufficient kinetic energy (proportional to v^2) to destroy the target (*18*).

Although the rotational light curve properties of the NEA population are consistent with the notion that the NEAs are entirely derived from the main belt, there is other physical and dynamical evidence suggesting that comet nuclei are indeed part of the NEA population (*5, 19*). Because comet nuclei have rotational properties that fall within the range observed for asteroids, these measurements do not rule out the presence of comet nuclei within the NEA population.

To quantify the problem, we postulate that a fraction f of the NEA population is comprised by comet nuclei and the remaining proportion $(1 - f)$ is derived from the main belt. For the sake of this analysis, we explicitly assume that the available sample of cometary nuclei is a reasonable representation of its population. Similarly, our small main-belt sample is assumed to represent its population. We perform our analysis by comparing the observed NEA samples for rotational frequency and corrected amplitude with constructed samples comprising f comet observations plus $(1 - f)$ small main-belt observations, where f is allowed to vary.

For each chosen value of f, we used a Student's t statistic to test the null hypothesis that the observed NEA sample mean is the same as that for our constructed sample. With a two-tailed rejection criterion set at the 95% confidence level, the null hypothesis is acceptable for f in the range of 0 to 25%. At the 99% confidence level, it is acceptable for f in the range of 0 to 40%. Stated in other words, our observed distributions are consistent with 0 to 40% of the NEA population being derived from dormant or extinct comet nuclei, with the largest proportion, 60 to 100%, of the NEA population being derived from the main belt. Thus, our observationally based results favor a main-belt asteroid source (*4*) for a majority of NEAs, with comets contributing a percentage smaller than the equal share suggested by Monte Carlo calculations (*5*).

REFERENCES AND NOTES

1. Approaching within 0.3 astronomical unit of the Earth.
2. E. M. Shoemaker, *Annu. Rev. Earth Planet. Sci.* **11**, 461 (1983); ______, R. F. Wolfe, C. S. Shoemaker, *Geol. Soc. Am. Spec. Pap.* **247** (1990).
3. L. W. Alvarez, W. Alvarez, F. Asaro, H. V. Michel, *Science* **208**, 1095 (1980).
4. J. Wisdom, *Icarus* **56**, 51 (1983); *Nature* **315**, 731 (1985).
5. G. W. Wetherill, *Icarus* **76**, 1 (1988).
6. E. M. Shoemaker, J. G. Williams, E. F. Helin, R. F. Wolfe, in *Asteroids*, T. Gehrels, Ed. (Univ. of Arizona Press, Tucson, 1979), pp. 253–282.
7. L. A. McFadden, D. J. Tholen, G. J. Veeder, in *Asteroids II*, R. P. Binzel, T. Gehrels, M. S. Matthews, Eds. (Univ. of Arizona Press, Tucson, 1979), pp. 442–467.
8. R. P. Binzel, *Icarus* **57**, 294 (1984); ______ and J. D. Mulholland, *ibid.* **56**, 519 (1983).
9. W. Z. Wisniewski, *ibid.* **90**, 117 (1991).
10. R. P. Binzel, S. Xu, S. J. Bus, E. Bowell, *ibid.*, in press.
11. C.-I. Lagerkvist, A. W. Harris, V. Zappalà, in *Asteroids II*, R. P. Binzel, T. Gehrels, M. S. Matthews, Eds. (Univ. of Arizona Press, Tucson, 1979), pp. 1162–1179.
12. D. Jewitt, in *Comets in the Post-Halley Era*, R. L. Newburn *et al.*, Eds. (Kluwer, Dordrecht/Boston, 1991), pp. 19–65; W. Z. Wisniewski, *Icarus* **86**, 52 (1990).
13. H. Karttunen and E. Bowell, *Astron. Astrophys.* **208**, 320 (1989).
14. V. Zappalà *et al.*, *ibid.* **231**, 548 (1990).
15. R. P. Binzel and L. M. Sauter, in preparation.
16. J. A. Burns, *Nature* **338**, 303 (1989).
17. We address the robustness of our results to the addition of new data. As a possible example of a new measurement, we take the cometary object 2060 Chiron located in the outer solar system. Its measured rotational properties are asteroidal [rotation = 5.92 hours, light-curve amplitude = 0.09 magnitude; S. J. Bus *et al.*, *Icarus* **77**, 223 (1989)], but were excluded because of its large diameter (>100 km). However, we find that adding it to the comet sample does not change the statistical

conclusions. To further investigate the robustness of our results, we presumed that the next three comets observed (thereby increasing the sample size by 60%) have the same rotational properties as Chiron. The one-tailed confidence level for the differences between the near-Earth and comet samples drops from >99% to 95%. For our conclusion that the NEA population is comprised by no more than 40% comet nuclei, the confidence level also drops from 99% to 95%. The robustness arises because the mean values for the current comet sample are so disparate from the asteroid samples that a comparable addition in the opposite tail is needed to offset the difference. Because new values are likely to be centered on the true mean, which is unlikely to be in the opposite tail, it will take a large increase in the sample size to significantly alter the sample mean.

18. R. P. Binzel, thesis, University of Texas, Austin (1986).
19. P. R. Weissman, M. F. A'Hearn, L. A. McFadden, H. Rickman, in *Asteroids II*, R. P. Binzel, T. Gehrels, M. S. Matthews, Eds. (Univ. of Arizona Press, Tucson, 1979), pp. 880–920.
20. Data reported in this paper were obtained in part at the Michigan Dartmouth MIT Observatory. This research was supported by National Science Foundation grant 88-18855 AST (R.P.B.), NASA grant NAGW-1470 (E.B.), and the Lowell Observatory endowment.

3 March 1992; accepted 25 June 1992

Uranium Bioaccumulation by a *Citrobacter* sp. as a Result of Enzymically Mediated Growth of Polycrystalline HUO_2PO_4

Lynne E. Macaskie,* Ruth M. Empson, Anthony K. Cheetham,† Clare P. Grey,‡ A. Jerome Skarnulis§

A *Citrobacter* sp. accumulates heavy deposits of metal phosphate, derived from an enzymically liberated phosphate ligand. The cells are not subject to saturation constraints and can accumulate several times their own weight of precipitated metal. This high capacity is attributable to biomineralization; uranyl phosphate accumulates as polycrystalline HUO_2PO_4 at the cell surface. The precipitated metal is indistinguishable from crystalline $HUO_2PO_4 \cdot 4H_2O$ grown by chemical methods.

A *Citrobacter* sp. accumulates heavy metals as a result of precipitation with enzymically liberated inorganic phosphate (*1, 2*). This reaction has been harnessed to a biotechnological process for the treatment of metal-bearing streams (*3, 4*); it also has potential for nuclear waste decontamination (*5*), facilitated by the high radioactive tolerance of the cell-bound phosphate-releasing enzyme (phosphatase) (*6*). The immobilized whole-cell biocatalyst tolerates loads of up to 9 g of accumulated uranium per gram of biomass (900% of the cellular dry weight) over several weeks without apparent ill effect (*4*). A packaging mechanism for the U might be postulated to permit enzyme turnover, yet the high toxicity of uranyl ion (*7*) makes a biochemical compartmentalization on this scale unlikely. With a continuous supply of organic phosphate donor molecules to cells immobilized in a flow-through cartridge ("bioreactor"), a steady state is rapidly achieved whereby metal is removed continuously and efficiently from the flow with a corresponding accumulation of metal within the bioreactor (*3*).

In this study we used electron microscopy to examine the mechanisms of metal accumulation and the fate of individual cells subjected to uranyl ion loading. The cells were not fixed or stained in any way, and, as such, before U challenge they were indistinct, and there was no accumulation of electron-dense material (Fig. 1A). Cells challenged in suspension with uranyl nitrate and phosphatase substrate for 12 hours accumulated U to about 250% of the bacterial dry weight (*8*) and were highly electron-opaque with little visible surface detail (Fig. 1B). Dried, ground samples of the loaded cells were lemon yellow in color and exhibited fluorescence characteristic of uranyl compounds. A video image of a cell revealed areas of enhanced electron opacity, primarily at the cell periphery (Fig. 1C), which we analyzed further by imaging for U (Fig. 1D) and phosphorus (Fig. 1E), using the x-ray emissions characteristic of these elements (U $L\alpha$ and P K).

Clear evidence for codeposition suggests that a form of uranium phosphate had been produced. X-ray microanalysis of specimen microareas (Fig. 1F) indicates that cells unchallenged with the uranyl ion showed x-ray emissions attributable to the low level of P associated with biological material, as well as the copper present in the grid. Qualitatively, the cellular deposit is indistinguishable from a hydrogen uranyl phosphate standard ($HUP{:}HUO_2PO_4 \cdot 4H_2O$) (Fig. 1F). Quantitative comparisons were made by integration of the areas under the U $L\alpha$ and P K peaks and were interpreted by the ratio method (*9*): $X_1/X_2 = kI_1/I_2$, where k is a constant and X_1, X_2, I_1, and I_2 represent, respectively, the concentrations and the emission intensities of the two elements. These data do not provide information on the absolute amounts of U and P accumulated, but the peak ratio can be used for comparison with the corresponding ratio obtained using the known atomic ratio of U to P in the HUP standard (U:P ratio = 1:1). The ratio of the peak areas for the standard was 1.91 ± 0.048, while that for the accumulated material was 1.75 ± 0.15 (mean $\pm$ standard errors from 15 and 10 determinations, respectively). These values are not significantly different at $P = 0.95$; taking into account that the cell also contains "biological" P (which would tend to reduce the peak area ratio), we conclude that the atomic U:P ratio in the cellular deposit is close to 1:1. However, this ratio could also be given by other uranium phosphates, and, as confirmation that HUP has indeed been formed, we examined the standard and accumulated material by solid-state infrared spectroscopy, x-ray diffraction, and magic angle spinning nuclear magnetic resonance (MASNMR).

The HUP standard was prepared by the method of Weigel and Hoffman (*10*), and its x-ray diffraction pattern was found to be in good agreement with the published data for HUP (*10, 11*). Infrared spectroscopy was performed in a carrier of cesium chloride at a weight:weight ratio of ground standard or ground U–loaded biomass to CsCl of 1:30. The spectra were very similar, with strong absorption peaks at 930 nm characteristic of the uranyl ion (*12*). We conclude that the accumulated material is a form of uranyl phosphate.

Further analyses with ^{31}P MASNMR indicated that proton-decoupled spectra from the U-loaded cells and the uranyl phosphate standard exhibit resonances at similar isotropic chemical shifts (σ_{iso} = 22.7 and 19.5 ppm, respectively) and have similar side-band intensities. Both the isotropic shift and the chemical shift anisotropy can be used to identify the phosphate species present. In general, pyrophosphates resonate upfield from the corresponding orthophosphate compounds (*13*), and hence the similar isotropic chemical shift for the uranyl phosphate standard and loaded cells confirmed that phosphate groups

L. E. Macaskie, School of Biological Sciences, University of Birmingham, Edgbaston, Birmingham, B15 2TT, United Kingdom.
R. M. Empson, Saint Mary's Hospital Medical School, Praed Street, London, W21NY, United Kingdom.
A. K. Cheetham, C. P. Grey, A. J. Skarnulis, Laboratory of Chemical Crystallography, University of Oxford, Parks Road, Oxford, OX1 3PD, United Kingdom.

*To whom correspondence should be addressed.
†Present address: Materials Department, University of California, Santa Barbara, CA 93106.
‡Present address: Molecular Spectroscopy Laboratory, Faculty of Physical Sciences, Toeerniveld, University of Nijmegen, Nijmegen, The Netherlands 6525 ED.
§Present address: Jeol Systems U.K. Ltd., Jeol House, Silver Court, Watchmead, Welwyn Garden City, Herts, AL7 1LT, United Kingdom.